ATLANTIS PRESS International Journal of Networked and Distributed Computing, Vol. 5, No. 2 (April 2017) 101–112

An Innovative Positioning System with Unsynchronized Interferometric Modulated Signals in Wireless Sensor Networks

Ruiling Gao [1], Alva Couch [2], Chorng Hwa Chang [3]

[1] *Department of Electrical and Computer Engineering, Tufts University,*
161 College Avenue
Medford, MA 02155, USA
E-mail: ruiling.gao@tufts.edu

[2] *Department of Computer Science, Tufts University,*
161 College Avenue
Medford, MA 02155, USA
E-mail: couch@cs.tufts.edu

[3] *Department of Electrical and Computer Engineering, Tufts University,*
161 College Avenue
Medford, MA 02155, USA
E-mail: hchang@ece.tufts.edu

Abstract

In this paper, we investigate the sensor localization problem and present Stochastic Radio Interferometric Positioning System with Unsynchronized Modulated Signals (SRIPS_UMS). Previous radio interferometric positioning methods have limitations include (1) strict hardware requirements for Received Signal Strength Indicator (RSSI) circuitry (2) time synchronization problem between distributed hardware. SRIPS_UMS overcomes these by using unsynchronized interferometric modulated signals. Its viability and advantages are demonstrated through mathematical models and extensive simulations. Further, the ongoing hardware implementation based on CC2420 is presented.

Keywords: sensor localization; radio interferometric positioning system; unsynchronized; CC2420

1. Introduction

Wireless Sensor Networks (WSN) have been attracting explosive interest from both academia and industry.[1, 2] Sensors have been deployed all over the world to collect and process vast amounts of data for various of civilian and military applications, such as smart city, weather sensing, and earthquake monitoring. Many wireless network applications depend on location information to get the context of the measured data or to provide support to network services (e.g. routing). Localization can also be a stand-alone application, such as navigation and target tracking. Sensor localization problem is one of the fundamental issues in WSN. Most traditional localization systems, such as Global Positioning System (GPS), are not suitable for WSN because sensors are resource-constrained.[3, 4] Compared with most existing localization systems, a qualified localization scheme for WSN additionally needs to have good scalability and low CPU/power/memory consumption.

In this paper, we focus on localization in static Wireless Sensor Networks in outdoor environment. Most current localization solutions are based on Received Signal Strength (RSS)[5, 6, 7] using an indicator of RSS called Received Signal Strength Indicator (RSSI) that is available on most sensor radio chips. However, much calibration and maintenance work are required and its accuracy is not always satisfactory. Other methods relying on Time Difference of Arrival (TDOA), Time of Flight (TOF), and Angle of Arrival (AOA) are more accurate than the RSS methods but need expensive specialized hardware.[8, 9] As a result, sensor localization remains a challenging problem.

Compared with the above localization methods, Radio Interferometric Positioning Systems (RIPS) offer high accuracy and long range simultaneously, without the requirement of special hardware. RIPS yields an average localization error of 3 cm within an area with a 160 m radius in outdoor environment.[10] Many efforts have been made to improve RIPS.[11, 12, 13, 14, 15] However, it is still difficult to implement RIPS algorithms on existing hardware:

- Many current radio chips have changed the design of RSSI circuitry.
- Resolution requirement of time synchronization cannot be achieved by many current sensor hardware.
- Mica2 is proven to be appropriate for RIPS/SRIPS implementation, but it is too old and is not available in the market now.
- Advanced sensors with direct phase measurement are not available in production.
- ZigBit with proper micro controller and radio chip is not supported in existing products; some pins may be not connected and neither Contiki nor TinyOS support it.
- None of the sensors supported by the latest version of Contiki and TinyOS has been proved.

Over the last decade, researchers have been focusing on improving RIPS with unmodulated signals with the ignorance of the fact that modulated signals with close carrier frequencies can still interfere with each other. Many experiments based on different sensor platforms have been conducted to study and model the interference phenomenon caused by concurrent packet transmissions in low-power sensor networks.[16, 17, 18] Moreover, it has been demonstrated in theory that RIPS using synchronized interferometric modulated signals is capable of positioning targets in the same way as previous RIPS methods utilizing unmodulated signals, with more benefits such as saving switching time.[15]

In this paper, we present Stochastic Radio Interferometric Positioning System with Unsynchronized Modulated Signals (SRIPS_UMS) – a variant of Stochastic RIPS[14] and Stochastic RIPS with Modulated Signals[15] that makes previous RIPS methods possible on existing hardware. Previous RIPS methods require sensor hardware to be able to continuously report RSS value, such as found on the CC1000.[19] They cannot be implemented on current mainstream hardware such as CC2420[20] and CC2520,[21] which instead report an average RSS value in every 128 us. Another problem is that previous methods using interferometric modulated signals require microsecond-level time synchronization on senders that is very hard to be realized on many sensor platforms. We need an innovative algorithm that can operate on the new-generation RSSI circuitry and also has much lower time synchronization requirements. Our improved algorithm SRIPS_UMS makes this possible and its viability is demonstrated theoretically through mathematical models and simulations. Direct Sequence Spread Spectrum Offset-Quadrature Phase Shift Keying (DSSS O-QPSK) modulation is used by many mainstream radio chips.[20, 21, 22] This modulation method is also utilized in mathematical models and simulations of this paper. In the hardware implementation plan, Zolertia Z1[23] with radio chip CC2420 is used. Hardware requirements for different RIPS methods are listed in Table 1.

Table 1. Hardware Requirements for RIPS Methods

	SRIPS	SRIPS_MS	SRIPS_UMS
Average RSS			√
Real-time RSS	√	√	
Unmodulation	√		

The major contributions of our work are:

- We introduce an innovative radio interferometric positioning system called SRIPS_UMS and theoretically demonstrate that it can be implemented on current mainstream radio chips that do not support previous RIPS methods.
- To the best of our knowledge, we are the first to utilize unsynchronized modulated signals for radio interferometric positioning and demonstrate its viability in theory.

- We theoretically demonstrate that it is not necessary for SRIPS_UMS to synchronize senders in time or to synchronize senders with receivers in time. Those time offsets almost have no affect on the positioning accuracy.
- We design a hardware implementation plan to implement a prototype of SRIPS_UMS.

The remainder of the paper is structured as follows. In section 2, we introduce SRIPS_UMS, including its mathematical models, related simulation results, and preliminary evaluation. In section 3, further simulation results and discussions are presented. Then in section 4 we show a hardware implementation plan based on CC2420. Finally, conclusions are given in section 5.

2. Stochastic Radio Interferometric Positioning System with Unsynchronized Modulated Signals

SRIPS_UMS utilizes radio interferometry of two unsynchronized modulated signals with nearby carrier frequencies to generate a composite signal with low frequency envelope for position estimation.

In this section, some problems of previous RIPS methods are first introduced. To solve these problems, we come up with SRIPS_UMS. Then we present the mathematical models and some preliminary evaluation results of SRIPS_UMS. Mathematical models are described in details to demonstrate the viability of SRIPS_UMS in theory, including signal modulation, signal propagation, signal interference, composite signal mix-down process, RSSI sampling, phase offset calculation, range, and positioning algorithm. A set of phase offsets are needed so that the positioning algorithm can converge to localize the target.

SRIPS_UMS is a combination of the SRIPS model and the SRIPS_MS model. SRIPS model uses unmodulated signals while SRIPS_MS model and SRIPS_UMS model are based on modulated signals. SRIPS_UMS model improves SRIPS_MS model by getting rid of the need to synchronize senders in time to microsecond resolution.

2.1. Hardware limitations

2.1.1 RSSI circuitry

One important hardware requirement for previous RIPS methods, including SRIPS_MS, is that the RSSI circuitry of receivers should be capable of reporting RSS values continuously. However, many current radio chips have abandoned this and instead only expose an average RSS value over 128 us. Although an obvious phase offset exists for actual RSS signals at the two receivers, the measured RSS-time curves are almost the same in phase due to the average process of RSSI circuitry. This will cause huge errors in estimating the target's position. There is an urgent need to improve traditional RIPS methods by resolving this problem.

2.1.2 Time synchronization

It has been demonstrated in theory that if senders are synchronized with receivers in microsecond accuracy, phase offset of RSS signals can be directly obtained from RSS values continuously measured by receivers[15] (as shown in Fig. 1). However, when the time synchronization requirement cannot be met, this relationship breaks up and a new strategy is needed, which is another motivation for us to come up with the following mathematical models using unsynchronized modulated signal for positioning a target.

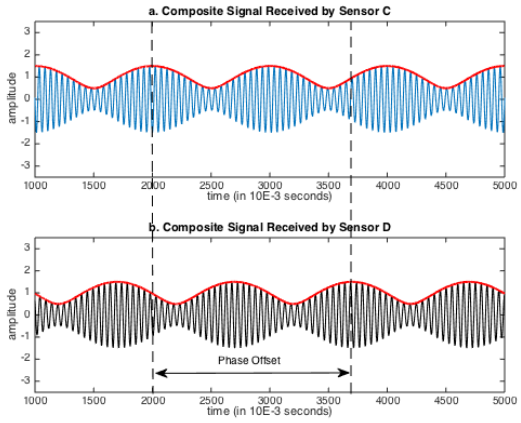

Fig. 1. Phase Offset Calculation with Time Synchronization

2.2. Mathematical models of SRIPS_UMS

At least four sensors are needed to position a target, with two as senders and the remaining ones as receivers. Only the target's position is unknown. Denote senders as A and B and receivers as C and D. D is the target. Let X be either A or B, and Y be either C or D. Denote the clock time of receivers as t and the clock time of senders as t_X. f_X is the carrier frequency of sender X and a_X is the signal amplitude.

Assumptions for mathematical models:

- Two receivers are synchronized in time and are listening simultaneously.
- Two senders are sending a same symbol sequence continuously.
- Symbol sequence is randomly formed from symbol 0~15.
- Senders are operating on the same channel in one phase offset measurement round.
- Two radios tuned to the same channel still have small and stable carrier frequency difference $f_A - f_B$ in a short period (let $f_A > f_B$).[14]
- Carrier frequency difference $f_A - f_B$ is less than 2 KHz.[10]

2.2.1 DSSS O-QPSK modulation with half-sine chip shaping

The modulation format in our mathematical models is DSSS O-QPSK with half-sine chip shaping, which is equivalent to Minimum-Shift Keying (MSK) modulation in mathematics.

In radio chip CC2420, each symbol (4 bits) is spread using the IEEE 802.15.4 spreading sequence to 32 chips and each chip is transmitted alternately in the I and Q channels.[20] One symbol period is 16 us. As shown in Fig. 2, the DSSS O-QPSK modulated signal is a summation of two signals available on I channel and Q channel respectively.

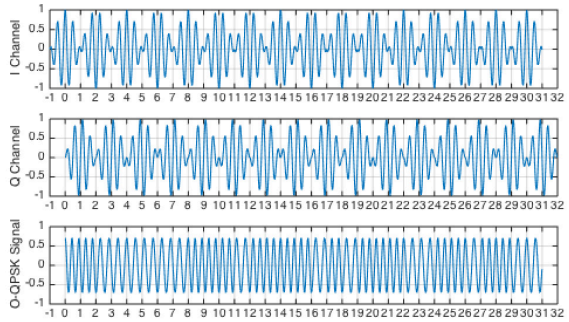

Fig. 2. DSSS O-QPSK Modulated Signal

For DSSS O-QPSK, the mathematical expression for the generated signal $S_{mod}(t_X)$ is:

$$S_{mod}(t_X) = \cos(2\pi f_X t_X + b_k(t_X)\frac{\pi t_X}{2T} + \varphi_k(t_X)) \quad (1)$$

, where $t_X = 0$ means the starting point when the sender X begins to send symbol sequence. $b_k(t_X)$ is +1 or -1 over time, and $\varphi_k(t_X)$ is 0 or π over time. The value of $b_k(t_X)$ and $\varphi_k(t_X)$ are controlled by chip values transmitted on I channel and Q channel.

2.2.2 Signal propagation

Denote the phase introduced by distance as φ_d. When the signal propagates for a wavelength in space, its phase changes for 2π. The changed phase is in proportion to the travel distance. The signal received at distance d can be expressed as:

$$S_{rec} = \cos\left(2\pi f_X t_X + b_k(t_X)\frac{\pi t_X}{2T} + \varphi_k(t_X) - \varphi_d\right) \quad (2)$$

2.2.3 Interference of modulated signals

Since in SRIPS_UMS senders are not required to be synchronized with each other or to be synchronized with receivers, time offsets may exist and can be expressed as:

$$t_X = t + \Delta t_X \quad (3)$$

In each phase offset measurement round, Δt_X is a constant and t_X is a variable. In different phase offset measurement rounds, Δt_X for a same sender/receiver pair can be a random constant and won't affect measurement results in theory, as demonstrated in section 3 through simulations.

The composite signal $S_Y(t)$ received by Y is the summation of the two signals, which can be expressed by Equation (4):

$$\begin{aligned} S_Y(t) = a_A\cos\Big(&2\pi f_A t_A + b_k(t_A)\frac{\pi t_A}{2T} + \varphi_k(t_A) \\ &- \varphi_{d_{AY}}\Big) \\ &+ a_B\cos\Big(2\pi f_B t_B + b_k(t_B)\frac{\pi t_B}{2T} \\ &+ \varphi_k(t_B) - \varphi_{d_{BY}}\Big) \end{aligned} \quad (4)$$

2.2.4 Mix down process of the composite signal

Sensor Y mixes down the composite signal $S_Y(t)$ with a local signal $m(t) = \cos(2\pi f_{LO} t)$. $m(t)$ is generated by a local oscillator and is used to convert the received signal to a resulting signal $S_Y^*(t)$ with an intermediate frequency f_{IF}. It can be expressed as:

$$S_Y^*(t) = S_Y(t)m(t) \quad (5)$$

Then $S_Y^*(t)$ is passed through a band pass filter to filter out the higher frequencies and to obtain the two low-frequency components. $f_A - f_B$ is very small compared with $b_k(t)/4T$ and f_{LO}. The resulting intermediate signal $S_{IF_Y}(t)$ only contains two signal

components with frequencies $f_A + b_k(t_A)/4T - f_{LO}$ and $f_B + b_k(t_B)/4T - f_{LO}$ separately. Set f_{LO} to $((f_A + f_B)/2) - f_{IF}$, let δ be $(f_A - f_B)/2$, and $S_{IF_Y}(t)$ can be written as:

$$S_{IF_Y}(t) = \frac{a_A}{2}\cos\Big(2\pi(f_{IF} + \frac{b_k(t_A)}{4T} + \delta)t + 2\pi(f_A + \frac{b_k(t_A)}{4T})\Delta t_A + \varphi_k(t_A) - \varphi_{d_{AY}}\Big) + \frac{a_B}{2}\cos\Big(2\pi(f_{IF} + \frac{b_k(t_B)}{4T} - \delta)t + 2\pi(f_B + \frac{b_k(t_B)}{4T})\Delta t_B + \varphi_k(t_B) - \varphi_{d_{BY}}\Big) \quad (6)$$

2.2.5 RSSI sampling

The signal power of $S_{IF_Y}(t)$ is:

$$S_{P_Y} = S^2_{IF_Y}(t) \quad (7)$$

Because RSSI measures RSS in dBm, a non-linear logarithmic function is used to read the RSS value. The logarithmic function distorts the composite signal by adding harmonic frequencies.[10] The harmonic frequencies can be filtered out by a properly designed low pass filter, leaving only the fundamental frequency. Hence we get the filtered RSS signal in dBm $S_{RSS_Y}(t)$:

$$S_{RSS_Y}(t) = \log\Big\{\frac{a_A^2 + a_B^2}{8} + \frac{a_A a_B}{4}\cos\Big[2\pi\Big(2\delta + \frac{b_k(t_A)}{4T} - \frac{b_k(t_B)}{4T}\Big)t + 2\pi\Big(f_A + \frac{b_k(t_A)}{4T}\Big)\Delta t_A - 2\pi\Big(f_B + \frac{b_k(t_B)}{4T}\Big)\Delta t_B + \varphi_k(t_A) - \varphi_k(t_B) - \varphi_{d_{AY}} + \varphi_{d_{BY}}\Big]\Big\} \quad (8)$$

We have theoretically derived the mathematical expression of the filtered RSS signal in dBm for composite unsynchronized modulated signals. It is a low-frequency signal.

From Equation (8), we can get raw RSS values $S_{Raw-RSS_Y}(t)$, as shown in Equation (9). Logarithm does not change the frequency and phase of signals. From now on, the filtered RSS signal refers to $S_{Raw-RSS_Y}(t)$ in this paper.

$$S_{Raw-RSS_Y}(t) = \frac{a_A^2 + a_B^2}{8} + \frac{a_A a_B}{4}\cos\Big[2\pi\Big(2\delta + \frac{b_k(t_A)}{4T} - \frac{b_k(t_B)}{4T}\Big)t + 2\pi\Big(f_A + \frac{b_k(t_A)}{4T}\Big)\Delta t_A - 2\pi\Big(f_B + \frac{b_k(t_B)}{4T}\Big)\Delta t_B + \varphi_k(t_A) - \varphi_k(t_B) - \varphi_{d_{AY}} + \varphi_{d_{BY}}\Big] \quad (9)$$

We simulate the waveform of the $S_{Raw-RSS_Y}(t)$, as shown in Fig. 3. The signal curve is not smooth and has a rough period as 2δ. 2δ is the carrier frequency difference that generally varies from 0 to several kilohertz. The frequency of $S_{Raw-RSS_Y}(t)$ contains a changing component $(b_k(t_A)/4T) - (b_k(t_B)/4T)$ that can be 1/2T, 0, or 1/2T over time. According to CC2420 data sheet, 1/2T equals to 1 MHz. When time changes and this component is 0, the frequency of the signal is 2δ. In other time periods when this equals to ±1 MHz, the signal's frequency becomes much larger and the signal's period becomes much shorter, with the same signal amplitude. This causes spikes on the curve of the filtered RSS signal in the time zone.

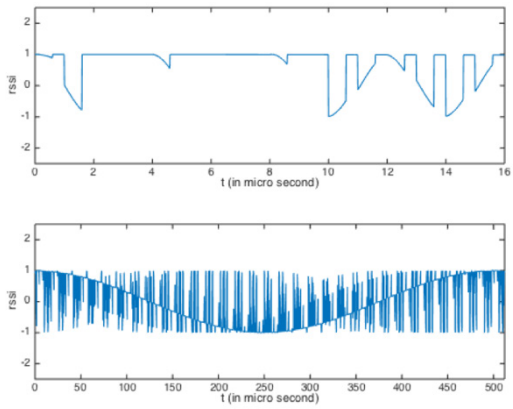

Fig. 3. Filtered RSS Signal in 1 Symbol Period and 32 Symbol Periods

If the user-defined measurement time for the filtered RSS signal is 20 ms, then the lower bound of the measurable frequency is 1/20 ms = 50 Hz. The Nyquist frequency determines the upper bound of the measurable frequency. In a RSSI circuitry with hardware sampling rate as 40 KHz, the upper bound is 40 KHz/2 = 20 KHz. However, for a RSSI circuitry that only exposes an average RSS reading every 128 us, the upper bound for the measurable frequency becomes much lower. Suppose we use such a RSSI circuitry to

measure a filtered RSS signal with a period of 128 us, the obtained RSS values will be almost the same and cannot be used to recover the filtered RSS signal. So it's reasonable to decrease the upper bound to $(1/128\ us) \approx 7.8$ KHz in this case. This average process won't affect the lower bound because it works like a smoothing process for filtered RSS signals with longer periods.

The phase of the filtered RSS signal contains distance information between involved sensors. The absolute phase is difficult to be measured, but the relative phase offset between two filtered RSS signals can be obtained and used for positioning.

2.2.6 Phase offset calculation

According to Equation (9), phase offset of filtered RSS signals at two receivers (sensor C and D) is:

$$\Delta\varphi = \left(\varphi_{d_{AD}} - \varphi_{d_{AC}}\right) + \left(\varphi_{d_{BC}} - \varphi_{d_{BD}}\right) \quad (10)$$

$\varphi_{d_{XY}}$ is the phase introduced by the distance between sender X and receiver Y with $\varphi_{d_{XY}} = 2\pi(\frac{d_{XY}}{c/f})$. c is the speed of light in free space. $\varphi_{d_{XY}}$ has a periodicity of 2π. So $\Delta\varphi$ can be further expressed in the form of distance relationships as:

$$\Delta\varphi = 2\pi\left(\frac{d_{AD} - d_{AC}}{c/f_A} + \frac{d_{BC} - d_{BD}}{c/f_B}\right) mod\ 2\pi \quad (11)$$

With radio chips that average RSS values over 128 us, the filtered RSS signal shown in Fig. 3 will be exposed in another form, as illustrated in Fig. 4. We call this curve "average-RSS-time curve" in this paper. From simulations in section 3, when carrier frequency difference $f_A - f_B$ is less than 2 KHz, average-RSS-time curve displays a rough periodicity and its period approximates to $1/(f_A - f_B)$ regardless of time offsets $(\Delta t_A, \Delta t_B)$.

In Fig. 4, 1600 symbol periods are taken to get 200 average RSSI readings, which equals to 25.6 ms. Another phase offset $\Delta\varphi_{Ave-RSS}$ is observed by comparing the two average-RSS-time curves measured by receiver C and receiver D respectively. In section 3, further simulation reveals the approximate relationship between $\Delta\varphi_{Ave-RSS}$ and $\Delta\varphi$ when the carrier frequency difference is low within 2 KHz range:

$$\Delta\varphi = \Delta\varphi_{Ave-RSS} \quad (12)$$

Since $\Delta\varphi_{Ave-RSS}$ can be measured, we obtain the value of $\Delta\varphi$. Substitute the value of $\Delta\varphi$ into Equation (11) to get the distance relationship.

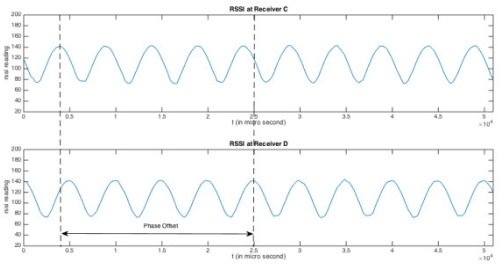

Fig. 4. Phase Offset of Two Average-RSS-Time Curves

2.2.7 Range

According to Theorem 3 in Ref. 10, if the carrier frequency difference is less than 2 KHz, Equation (11) can be rewritten as:

$$\Delta\varphi = 2\pi\left(\frac{d_{AD} - d_{AC} + d_{BC} - d_{BD}}{c/f}\right) mod\ 2\pi \quad (13)$$

, where $f = (f_A + f_B)/2$.

Define q_{range} as:

$$q_{range} = d_{AD} - d_{AC} + d_{BC} - d_{BD} \quad (14)$$

Sensor A, B, and C's locations are known, so d_{AC} and d_{BC} can be calculated. Equation (14) can be further expressed in the form of t_{range}:

$$t_{range} = q_{range} + d_{AC} - d_{BC} = d_{AD} - d_{BD} \quad (15)$$

One iteration of the above process is called a "phase offset measurement round". Repeat the phase offset measurement for different frequency channels and we can estimate q_{range} based on a "least common multiple" approach mentioned in Ref. 10. A more advanced and accurate solution for q_{range} estimation is to use "Chinese Remainder Theorem".[24, 25]

After q_{range} is obtained, t_{range} can be calculated using Equation (15). From the definition of hyperbola, it is known that target D is actually located on one branch of the hyperbola with two foci as the locations of sensor A and sensor B. Then repeat phase offset measurements with sensor A and C as senders and sensor B and D as receivers. A new t_{range} can be calculated and it equals to the difference between the distance of the target and sensor A and the distance of the target and sensor C. So target D is also on one branch of another hyperbola with two foci as the locations of sensor A and sensor C. The intersection of two hyperbola branches is the estimated target position, as illustrated in Fig. 5.

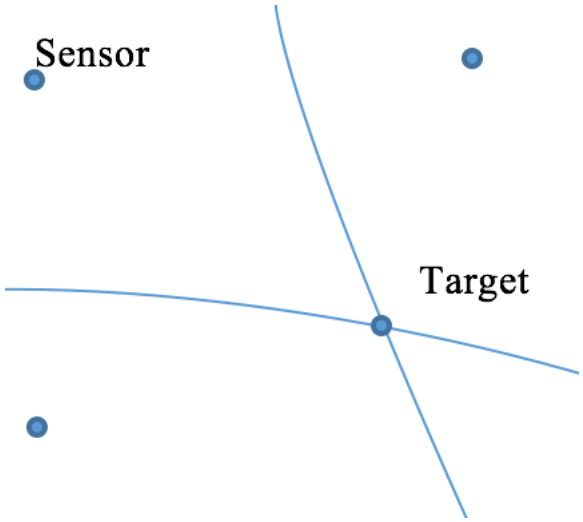

Fig. 5. Tracking a Single Target with Intersections of Hyperbolic Curves

However, for a radio chip operating on 2.4 GHz band with frequency accuracy ±40 ppm, the maximum frequency offset can reach up to 200 KHz.[20] As a result, the actual carrier frequency difference can be much larger than 2 KHz. This will bring in unestimated errors in range calculation and add much complexity to mathematical models. It is necessary to find a solution to distinguish effective measurements with carrier frequency differences in the range of 2 KHz and discard those noneffective measurements beyond the scope. In section 3, simulation results show that obvious visual differences exist for the shape of average-RSS-time curves under different carrier frequency differences. This provides a clue for us to utilize some characteristics of the average-RSS-time curve to tell whether the measurement is effective or not. But further careful and in-depth research are needed to make solid and convincing conclusions.

2.2.8 Stochastic radio interferometric positioning algorithm

Instead of using the range-based positioning algorithm mentioned above, we prefer to utilize the stochastic positioning algorithm in Ref. 14 that can eliminate false global optimums and converge more accurately to true locations. In this algorithm, a set of phase offsets obtained under different carrier frequencies and different sender/receiver pair combinations are input into the below equation to find the optimal target position (x_D, y_D) with best fit:

$$(x_D, y_D) = \arg min_{(x_D, y_D)} \sum_{j=1}^{M} \sum_{i=1}^{N} \left(\Delta\varphi_{i,j} - \Delta\varphi_{i,j}^{*}\right)^2 \quad (16)$$

, where $\Delta\varphi_{i,j}$ is the measured phase offset for carrier frequency f_i under sender/receiver pair combination j. $\Delta\varphi_{i,j}^{*}$ is the actual phase offset in the same scenario. As shown in Equation (16), obtaining precise phase offsets is critical for accurate position estimation. According to Equation (13), if we assume sensor A and B are senders in combination j with locations (x_A, y_A) and (x_B, y_B) respectively, $\Delta\varphi_{i,j}^{*}$ can be expressed as:

$$\Delta\varphi_{i,j}^{*} = 2\pi \left(\frac{d_{AD} - d_{AC} + d_{BC} - d_{BD}}{c/f_i}\right) mod\ 2\pi \quad (17)$$

Since only sensor D's location is unknown, d_{AC} and d_{BC} can be calculated. d_{AD} and d_{BD} can be expressed using sensors' locations:

$$d_{AD} = \sqrt{(x_A - x_D)^2 + (y_A - y_D)^2} \quad (18)$$

$$d_{BD} = \sqrt{(x_B - x_D)^2 + (y_B - y_D)^2} \quad (19)$$

2.3. Preliminary evaluation of SRIPS_UMS

2.3.1 Switching time

SRIPS_UMS saves switching time. According to the positioning process described in Ref. 10 and Ref. 14, sensors use unmodulated signals for phase offset measurements and they also need to switch to modulation mode for communication purpose, such as receiving scheduling commands for localization. Denote the switching time as t_s and the number of switching is N, then the total saved localization time is $N \times t_s$, where t_s is defined by radio chip data sheet.[20, 21, 22]

2.3.2 Noise analysis

In Ref. 15, it is pointed out that RIPS using modulated signals theoretically performs better than other RIPS methods with unmodulated signals in noisy environments. We expect SRIPS_UMS to inherit this advantage.

Obviously, noise from other than the carrier frequencies is rejected by the transceiver. So we're only concerned with noise that gets through the filter. The noise that gets through is not white; it is "pink" in the sense that it is concentrated in specific frequency bands.

2.3.3 Error sources

Some major error sources of SRIPS_UMS include:

- Carrier frequency drift: sensor's frequency can drift and effect phase offset measurements.
- Noise: the noise from other wireless networks operating on the same channel, such as the ubiquitous Wi-Fi network.

- Data processing: errors introduced by algorithms that calculate phase offsets.
- Time synchronization of receivers: it's important for receivers to establish time synchronization points with high resolution to ensure accurate phase offset measurements.

3. Simulation Results

In this section, we conduct extensive simulations to study average-RSS-time curves in terms of the waveform, period, and phase offset. Results provide supports for Equation (12) and thus demonstrate the viability of SRIPS_UMS on new-generation radio chips. And we also prove another important advantage of SRIPS_UMS that it doesn't need time synchronization on sender side. From simulations, time offsets $(\Delta t_A, \Delta t_B)$ can be arbitrary and they have very little affect on positioning accuracy.

A simple scenario is used in our simulations. We consider a square field 20×20 m with 4 sensors deployed in outdoor environment. The target sensor is the only one with unknown position in each phase offset measurement round and its role is always receiver.

3.1. Carrier frequency difference and its effects on average-RSS-time curve

Carrier frequency differences pose very obvious visual effects on the shape of averaged-RSS-time curves, as shown in Fig. 6. X-axis is time and Y-axis is signal amplitude. The Y-axis of Fig. 6 (a)~(h) has the same range from 20 to 200.

With the increase of the carrier frequency difference, the amplitude of average-RSS-time curve decreases. When the carrier frequency difference is under 2 KHz, the average-RSS-time curve displays a rough periodicity. Compared with these curves, average-RSS-time curves with much higher carrier frequency differences (20 KHz and 200 KHz) look like horizontal lines without any periodicity.

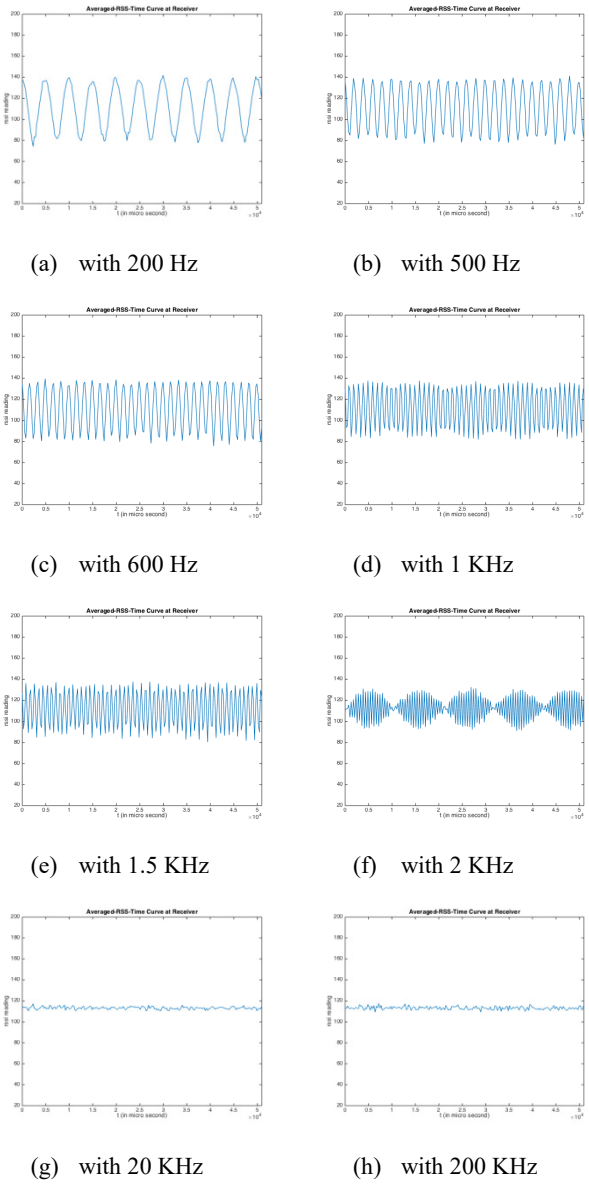

(a) with 200 Hz (b) with 500 Hz

(c) with 600 Hz (d) with 1 KHz

(e) with 1.5 KHz (f) with 2 KHz

(g) with 20 KHz (h) with 200 KHz

Fig. 6. Average-RSS-Time Curves with Different Carrier Frequency Differences

3.2. Time offsets and average period of average-RSS-time curve

The estimation for the frequency and phase of sine waves is a well-studied problem.[26, 27] In this paper, we define a period as the distance between three sequential peaks that is shown as the distance between two red adjacent dash lines in Fig. 7. In Fig. 7, the upper subplot is the average-RSS-time curve of our interest, and the lower one uses RSS in dBm instead of raw RSS values. Actually the defined period is not a constant for a same average-RSS-time curve, so an average value is calculated and used.

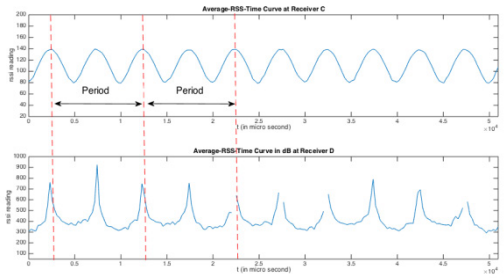

Fig. 7. Period of Average-RSS-Time Curves

Simulations are performed under different carrier frequency differences from 200 to 2000 Hz. X-axis is Δt_A and Y-axis is Δt_B. Z-axis is the measured period of average-RSS-time curve under time offsets $(\Delta t_A, \Delta t_B)$.

In Fig. 8 (a), although $(\Delta t_A, \Delta t_B)$ are changing, the average period of average-RSS-time curve remains around 5 ms. 5 ms is the reciprocal of the carrier frequency difference $f_A - f_B$ (200 Hz). Repeat this experiment under different carrier frequency differences (400 Hz~2000 Hz) and these results hold, as shown in Fig. 8 (b)~(f).

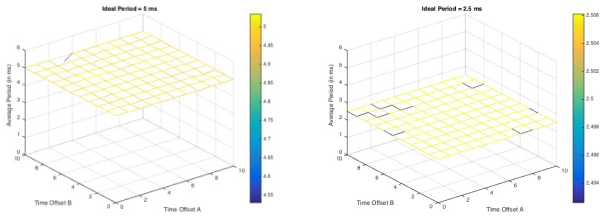

(a) $f_A - f_B$=200 Hz (b) $f_A - f_B$=400 Hz

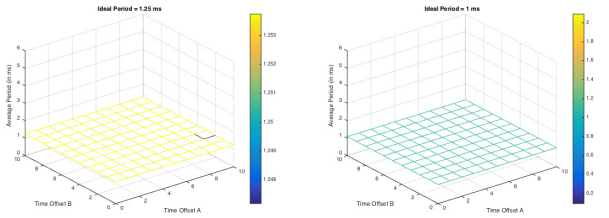

(c) $f_A - f_B$=800 Hz (d) $f_A - f_B$=1 KHz

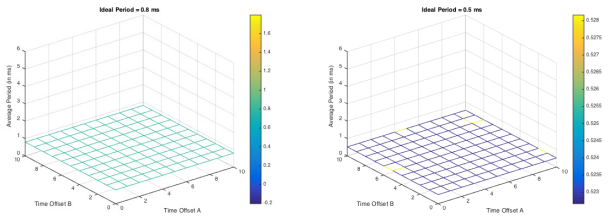

(e) $f_A - f_B$=1.25 KHz (f) $f_A - f_B$=2 KHz

Fig. 8. Average Period of Average-RSS-Time Curve under Different Time Offsets

3.3. Time offsets and phase offset of average-RSS-time curves

The phase offset of average-RSS-time curves is defined as an average value of the phase shifts between two adjacent peaks of the two average-RSS-time curves, as shown in Fig. 9.

We simulate the average-RSS-time curves measured by two receivers with changing time offsets. Results are available in Fig. 10 (a)~(h). X-axis is Δt_A and Y-axis is Δt_B. Z-axis is the measured phase offset between two average-RSS-time curves under time offsets $(\Delta t_A, \Delta t_B)$.

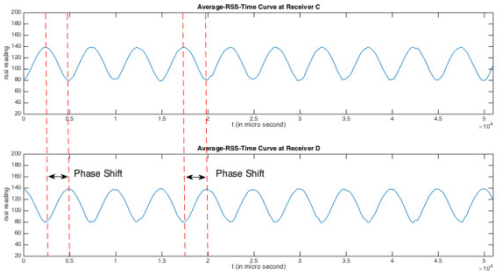

Fig. 9. Phase Offset of Average-RSS-Time Curves

In Fig. 10 (a), simulation is performed when phase offset of filtered RSS signals $(\Delta\varphi)$ is 0.2π, and the measured phase offset of average-RSS-time curves $\Delta\varphi_{Ave-RSS}$ stays around 0.2π under different time offsets $(\Delta t_A, \Delta t_B)$. Repeat this experiment under different $\Delta\varphi$, $\Delta\varphi_{Ave-RSS}$ still approximates to $\Delta\varphi$, as shown in Fig. 10 (b) (c) (d). Simulation results show that time offsets $(\Delta t_A, \Delta t_B)$ have very little effect on the value of $\Delta\varphi_{Ave-RSS}$ and $\Delta\varphi_{Ave-RSS}$ always approximates to $\Delta\varphi$.

The above mathematical models and simulations assume that senders are continuously sending random symbols chosen from symbol 0~15. There is a special case that the symbol sequence contains a codon (a piece of small symbol sequence that appears repeatedly). The effects of codon are simulated by using a long sequence of symbol 0. In reality, this can be achieved by continuously sending a same packet. We repeat the experiments with a codon sequence and results are available in Fig. 10 (e)~(h). Obtained conclusions are the same with the ones made in random sequence scenario.

X-axis of Fig. 10 (i)~(l) is time offset pair $(\Delta t_A, \Delta t_B)$. Y-axis the error in estimating $\Delta\varphi$. In Fig. 10 (i), we compare the results shown in Fig. 10 (a) and Fig. 10 (e) by calculating the errors (in Radians) of phase offset estimation in both scenarios. Other comparisons under different $\Delta\varphi$ are available in Fig. 10 (j)~(l).

The comparison results are summarized in Table 2. Compared with using random symbol sequence, utilizing codon sequence produces errors with higher mean and lower standard deviation in phase offset estimation.

Table 2. Mean and Standard Deviation of Errors in Radians for Phase Offset Estimation

	$\Delta\varphi = 0.2\pi$	04π	0.6π	0.8π
Mean	-0.0023	0.0015	-0.0015	0.0024
Mean (w/ codon)	0.0151	0.0302	0.0189	0.0121
Std	0.0371	0.0344	0.0322	0.0325
Std (w/ codon)	0	0	0.0078	0

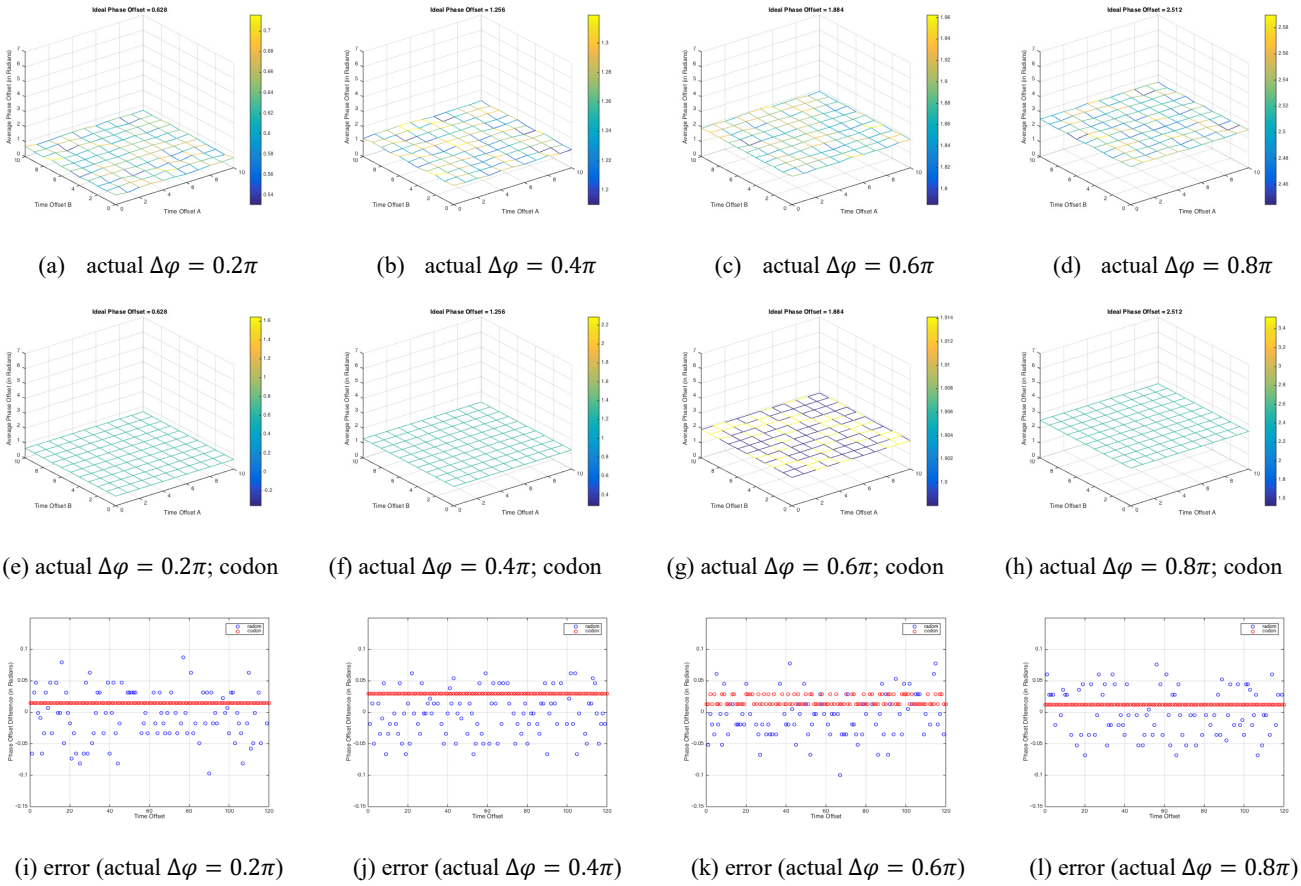

(a) actual $\Delta\varphi = 0.2\pi$ (b) actual $\Delta\varphi = 0.4\pi$ (c) actual $\Delta\varphi = 0.6\pi$ (d) actual $\Delta\varphi = 0.8\pi$

(e) actual $\Delta\varphi = 0.2\pi$; codon (f) actual $\Delta\varphi = 0.4\pi$; codon (g) actual $\Delta\varphi = 0.6\pi$; codon (h) actual $\Delta\varphi = 0.8\pi$; codon

(i) error (actual $\Delta\varphi = 0.2\pi$) (j) error (actual $\Delta\varphi = 0.4\pi$) (k) error (actual $\Delta\varphi = 0.6\pi$) (l) error (actual $\Delta\varphi = 0.8\pi$)

Fig. 10. Phase Offsets of Average-RSS-Time Curves with Different Time Offsets

4. Hardware Implementation

The positioning experiments will be conducted in a 20×20 m outdoor environment (as illustrated in Fig. 11), with five Zolertia Z1 sensors equipped with CC2420. The embedded operating system - TinyOS 2.1.2 is adopted for SRIPS_UMS implementation. We choose the target-as-receiver implementation because it has better scalability compared with the target-as-sender implementation.

To localize the target, several rounds of phase offset measurements are needed. CC2420 has 16 channels within the 2.4 GHz band, in 5 MHz steps. The receiving sensors obtain 200 RSSI readings per phase offset measurement in 25.6 ms per frequency over a total of 16 frequencies in a range of 2405 MHz to 2480 MHz. All RSSI readings will be sent to a personal computer (PC) and logged for further data processing and analysis.

Fig. 11. Deployment Area

4.1. Module design

We design software modules based on TinyOS for SRIPS_UMS:

- Sender: continuously send a same packet with adjustable packet length/packet interval/power level/communication channel
- Receiver: continuously listen on the radio communication channel and read RSS values from register
- Base Station: collect data from sensors and transmit them to PC; work as a gateway between the sensor network and outside networks, such as the Internet
- Time Synchronization Partner: synchronize sensors using Flooding Time Synchronization Protocol[28]
- Query: periodically send queries to the sensor network for synchronization progress
- Scheduler: schedule events with pre-defined time intervals

In the setup shown in Fig. 12, software module "Sender" is installed on both senders, while both receivers have the code of "Receiver" and "Time Synchronization Partner". Besides, the receiver connecting to PC is installed with the module "Base Station" additionally. Modules "Query" and "Scheduler" are installed on one sensor that can reach every other sensor in the network. The process to locate the target with SRIPS_UMS is illustrated in Algorithm 1.

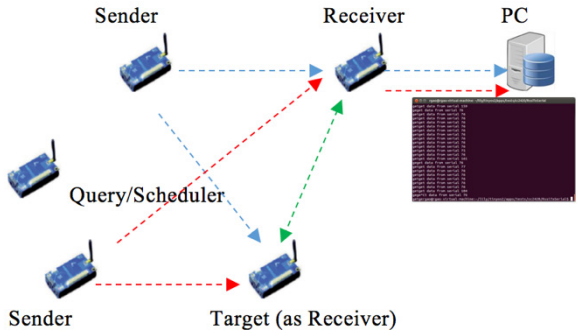

Fig. 12. Scheme of Communication in Z1 Sensor Network

4.2. Hardware implementation challenges

The first hardware implementation challenge is to turn off collision avoidance on sensors for the generation of signal interference. Although TinyOS wiki provides a standard solution to disable Clear Channel Assessment (CCA) for CC2420, careful verifications on hardware are needed to confirm the behavior.

Another problem is the time synchronization of receivers. The accuracy and stability of it will effect the performance of SRIPS_UMS. Assuming a 200 Hz interference frequency and a time synchronization with 2 us precision, this translates to $4\% \times 2\pi$ phase offset error. Many details are involved in the design.

Algorithm 1 SRIPS_UMS Algorithm

Input: sender and receiver pairs p_i $(i = 0, ..., m)$; communication channels f_j $(j = 0, ..., n)$; anchor nodes' positions (x_k, y_k) $(k = 0, ..., l)$
Output: target's position (x_t, y_t)
for p_i $(i = 0; i++)$
  for f_j $(j = 0; j++)$
    "Scheduler" schedules receivers to synchronize time;
    "Query" periodically ask for synchronization progress;
    while (synchronization is not finished)
      two receivers continue to synchronize;
    end while
    "Scheduler" schedules two senders start;
    "Receiver" collects RSS values;
    "Base Station" collects data and pass them to PC;
    PC calculates $\Delta\varphi_{(i,j)}$;
  end for
end for
use $\varphi_{i,j}$ to find a optimal (x_t, y_t) that minimizes $\Sigma_{j=1}^{M}\Sigma_{i=1}^{N}(\Delta\varphi_{(i,j)} - \Delta\varphi_{D(i,j)})^2$;

5. Conclusions

In this paper, we have described, evaluated, and partially implemented an innovative RIPS method - SRIPS_UMS. SRIPS_UMS theoretically resolves the hardware implementation problem of previous RIPS methods. And as a RIPS method utilizing modulated signals, it does not need time synchronization on senders or time synchronization between senders and receivers. The key enabling ideas behind these results are:

- The successful mathematical derivation of the filtered RSS signal.
- The discovery of the relationship between the phase offset of filtered RSS signals and the phase offset of average-RSS-time curves.
- Extensive simulation on the effects of time offsets regarding phase offset estimation that determines positioning accuracy.

Future work includes continuing work on hardware implementation of SRIPS_UMS on CC2420 and research on SRIPS_UMS utilizing new observations for possible indoor applications.[29]

Acknowledgement

The authors would like to thank every Tufts Wireless Lab (TWL) member for helpful discussions. Special thanks to Prof. Kyle Jamieson from Princeton University for the inspirational comments on this work. We also feel very grateful to Qingqian Liu for helping us photograph the sensor deployment field well.

References

1. L. Zhang, Q. Cheng, Y. Wang, and S. Zeadally, "A novel distributed sensor positioning system using the dual of target tracking," *IEEE Transactions on Computers*, vol. 57, no. 2, (2008), pp. 246–260.
2. R. Gao, M. Zhao, Z. Qiu, Y. Yu, and C. H. Chang, "Web-based motion detection system for health care," in *IEEE/ACIS 14th International Conference on Computer and Information Science*, (2015), pp. 65–70.
3. K. T. Kim, M. Y. Kim, J. H. Choi, and H. Y. Youn, "An energy efficient clustering algorithm for maximizing the lifetime of wireless sensor network," *International Journal of Networked and Distributed Computing*, (2015), pp. 214–223.
4. Y. Dong, C. H. Chang, and Z. Yang, "An improved autonomous cross-layer optimization framework for wireless multimedia communication in heterogeneous networks." *International Journal of Networked and Distributed Computing*, vol. 2, no. 4, (2014), pp. 231–240.
5. K. Aamodt, "CC2431 location engine," *Application Note AN042*, (2006), Texas Instruments.
6. A. Faheem, R. Virrankoski, and M. Elmusrati, "Improving rssi based distance estimation for 802.15. 4 wireless sensor networks," in *IEEE International Conference on Wireless Information Technology and Systems*, (2010), pp. 1–4.
7. M. A. A. A. Mazlan, M. H. M. Khir, and M. N. M. Saad, "Implementation of wireless sensor network in oil and gas specifically for personnel positioning application," in *IEEE International Conference on Computer, Communications, and Control Technology*, (2015), pp. 232–236.
8. R. Dalce, A. Van den Bossche, and T. Val, "Indoor self-localization in a wsn, based on time of flight: Propositions and demonstrator," in *International Conference on Indoor Positioning and Indoor Navigation*, (2013), pp. 1–6.
9. P. Rong and M. L. Sichitiu, "Angle of arrival localization for wireless sensor networks," in *3rd annual IEEE communications society on sensor and ad hoc communications and networks*, vol. 1, (2006), pp. 374–382.
10. M. Maróti, P. Völgyesi, S. Dóra, B. Kusy, A. Nádas, Á. Lédeczi, G. Balogh, and K. Molnár, "Radio interferometric geolocation," in *Proceedings of the 3rd international conference on embedded networked sensor systems*. ACM, (2005), pp. 1–12.
11. B. Kusy, A. Ledeczi, M. Maroti, and L. Meertens, "Node density independent localization," in *Proceedings of the 5th international conference on Information processing in sensor networks.* ACM, (2006), pp. 441–448.
12. H.-j. Wu, H.-l. Chang, C.-w. You, H.-h. Chu, and P. Huang, "Modeling and optimizing positional accuracy based on hyperbolic geometry for the adaptive radio interferometric positioning system," in *International Symposium on Location and Context-Awareness*. Springer, (2007), pp.228–244.
13. A. Ledeczi, P. Volgyesi, J. Sallai, B. Kusy, X. Koutsoukos, and M. Maroti, "Towards precise indoor RF localization," in *proc. of the 5th Workshop on Embedded Networked Sensors*, Charlottesville: ACM, (2008).
14. B. Dil and P. J. Havinga, "Stochastic radio interferometric positioning in the 2.4 GHz range." in *SenSys*, (2011), pp. 108–120.
15. R. Gao, Z. Yang, W.-T. Sun, C. H. Chang, and A. Couch, "Radio interferometric positioning with modulated signals in wireless sensor networks," in *111th International Conference on Communication and Signal Processing*, Japan, (2017).
16. D. Son, B. Krishnamachari, and J. Heidemann, "Experimental study of concurrent transmission in wireless sensor networks," in *Proceedings of the 4th international conference on Embedded networked sensor systems.* ACM, (2006), pp. 237–250.
17. R. Maheshwari, S. Jain, and S. R. Das, "A measurement study of interference modeling and scheduling in low-power wireless networks," in *Proceedings of the 6th ACM conference on Embedded network sensor systems*. ACM, (2008), pp. 141–154.
18. R. Maheshwari, S. Jain, and S. R. Das, "On estimating joint interference for concurrent packet transmissions in low power wireless networks," in *Proceedings of the third ACM international workshop on Wireless network testbeds, experimental evaluation and characterization*. ACM, (2008), pp. 89–94.
19. A. Chipcon, "CC1000 data sheet," 2004.
20. T. Instruments, "CC2420: 2.4 ghz ieee 802.15. 4/zigbee-ready rf transceiver," *Available at http://www. ti. com/lit/gpn/cc2420*, vol. 53, (2006).
21. T. Instruments, "CC2520 datasheet," (2007).
22. T. Instruments, "CC2430 data sheet," (2008).
23. W. Zolertia, "platform, z1 datasheet."
24. C. Wang, Q. Yin, and W. Wang, "An efficient ranging method based on Chinese remainder theorem for rips measurement," *Science China Information Sciences*, vol. 53, no. 6, (2010), pp. 1233–1241.
25. C. Wang, Q. Yin, and H. Chen, "Robust Chinese remainder theorem ranging method based on dual-frequency measurements," *IEEE Transactions on Vehicular Technology*, vol. 60, no. 8, (2011), pp. 4094–4099.
26. D. Rife and R. Boorstyn, "Single tone parameter estimation from discrete-time observations," *IEEE Transactions on information theory*, vol. 20, no. 5, (1974), pp. 591–598.
27. S. Tretter, "Estimating the frequency of a noisy sinusoid by linear regression", *IEEE Transactions on Information theory*, vol. 31, no. 6, (1985), pp. 832–835.
28. M. Maróti, B. Kusy, G. Simon, and Á. Lédeczi, "The flooding time synchronization protocol," in *Proceedings of the 2nd international conference on Embedded networked sensor systems*. ACM, (2004), pp.39–49.
29. J. Xiong and K. Jamieson, "Array track: A fine-grained indoor location system." in *NSDI*, (2013), pp. 71–84.